Li local environments and the dynamics in the $Li_{1+x}V_3O_8$ insertion electrode

2005 J. Phys.: Condens. Matter 17 4057

(http://iopscience.iop.org/0953-8984/17/26/006)

INSTITUTE OF PHYSICS PUBLISHING JOURNAL OF PHYSICS: CONDENSED MATTER

J. Phys.: Condens. Matter **17** (2005) 4057–4071 doi:10.1088/0953-8984/17/26/006

Li local environments and the dynamics in the $Li_{1+x}V_3O_8$ insertion electrode

Masashige Onoda[1], **Shintaro Miyasaka**[1], **Tomohiro Mutoh**[1] **and Katsuhiro Nichogi**[2]

[1] Institute of Physics, University of Tsukuba, Tennodai, Tsukuba 305-8571, Japan
[2] Tokyo Branch, Matsushita Electric Industrial Co., Ltd, Shibakoen, Minato-ku, Tokyo 105-8581, Japan

E-mail: onoda@sakura.cc.tsukuba.ac.jp

Received 2 May 2005, in final form 3 June 2005
Published 17 June 2005
Online at stacks.iop.org/JPhysCM/17/4057

Abstract

The structural and electronic properties of the $Li_{1+x}V_3O_8$ insertion electrode system with *nominal* range of $0 \leqslant x \leqslant 4.6$ have been explored through measurements of x-ray diffraction, magnetization and nuclear magnetic resonance (NMR) for ^{7}Li. The system prepared electrochemically exhibits two kinds of phase depending on the composition: the $\gamma 1$-phase with $0 \leqslant x \leqslant 1.5$ has the octahedral (Li1) and tetrahedral (Li2) coordinations for the Li sites, and the $\gamma 2$-phase with $x \geqslant 3.5$ has the octahedral coordination alone. These phases coexist for $1.5 < x < 3.5$. Application of the one-dimensional chain model to the susceptibility data for the $\gamma 2$-phase provides reasonable results for the Li concentration and the exchange constant. For $x = 0$, the quadrupole parameters are determined precisely. Both the $\gamma 1$-phase and the $\gamma 2$-phase indicate the activation energies for the long-range motion of Li ions to be of 3×10^3 K at temperatures above 300 K, and the $\gamma 2$-phase has another narrowing process below 100 K. Magic-angle spinning (MAS) NMR spectra for the $\gamma 1$-phase reflect the site differentiation for Li; the Li1 shift originates from a negative spin transfer, while the effect for Li2 is less significant. The spin-lattice relaxation for $x = 0$ is explained with the quadrupole interaction mechanism. For $Li_{1.25}V_3O_8$, which exhibits variable-range hopping-type transport anomalies at $T_c \simeq 250$ K, the phase transition for the Li local environments takes place at around T_c. The spectra for the $\gamma 2$-phase are different from those for the $\gamma 1$-phase, and the complicated relaxations likely originating from Li ions located in the cathode and the acetylene black, and the boundary between these substances, are observed.

1. Introduction

Various properties of transition-metal oxide systems have been investigated from the viewpoints of basic as well as applied sciences. The insertion electrode system that has recently received considerable attention is one of the applied sciences. $Li_{1+x}V_3O_8$ and $Li_xV_6O_{13}$ are typical systems for vanadium oxides that have such properties [1–8]. The former system can accommodate around three or four additional Li ions per formula unit of LiV_3O_8 [2] and the latter system eight ions per V_6O_{13} [7]. These lithiations may supply a new kind of compound series for the investigations of quantum-spin fluctuation and correlated electron systems. In order to construct this situation and to improve battery performances, it is important to study the basic properties as a function of the Li concentration, although the crystal structures for this system are rather complicated as compared with those for the well known insertion electrode systems.

The structural and electronic properties of $Li_{1+x}V_3O_8$ with $0 \leqslant x < 0.4$ and of the isomorphous systems $Na_{1+x}V_3O_8$ with $0.1 \leqslant x \leqslant 0.35$ and $Ag_{1+x}V_3O_8$ with $0.2 \leqslant x \leqslant 0.35$ were investigated by the authors' group [5, 6]. Here, the concentration ranges for M = Li, Na and Ag were determined with the solid-state reaction method. Figure 1(a) shows the crystal structure of $Li_{1.29}V_3O_8$, which is a typical compound for these systems. There exist three crystallographically independent V sites labelled V1, V2 and V3. The V1 ions have a pyramidal coordination, while the V2 and V3 ions have octahedral coordinations. The chains of VO_6 octahedra and those of VO_5 pyramids extending along the *b*-axis are linked by corner-shared oxygens to form continuous sheets of V–O polyhedra, that is a V_3O_8 framework. The networks for the equivalent sites of V1 and V2 are expressed as zigzag chains and that for the V3 site is a one-dimensional chain. The M ions are located predominantly in an octahedral site (M1) with a full occupancy and the excess xM ions reside in a tetrahedral site (M2) with some probability. The M2 sites with a symmetry-related M2–M2 distance of about 2 Å cannot be occupied simultaneously due to the strong Coulomb repulsion. Therefore, for M1 and M2 sites alone, the composition of $M_{1+x}V_3O_8$ is limited to $x = 0.5$. A significant difference of the crystal structures of $M_{1+x}V_3O_8$ with M = Li, Na and Ag is seen for the M–O and M–M distances. The M–O distance is understood in terms of the ionic radii of M and O. The M–M distance for the Ag system is very short, suggesting that it is the most unstable of these systems. In effect, the charge–discharge process in $Ag_{1+x}V_3O_8$ with negative electrode of Li metal exhibits the irreversible property accompanied with a deposition reduction of Ag ions. This is attributed to the difference of Li and Ag ionic radii; that is, the Li insertion for the Ag system forces the Ag–O distance to be short.

All of the $M_{1+x}V_3O_8$ systems described above exhibit the preferential and partial reduction of V ions: that is, most of the donated electrons are located at the V3 site, leading to low-dimensional electronic properties [5, 6]. LiV_3O_8 shows a quasi-one-dimensional polaronic transport in the localized states of band tails due to the slight deficiency of oxygen atoms. For $x \neq 0$, the conduction may be of variable-range hopping (VRH) type in one or three dimensions, mainly caused by the randomness of M2. Here, the dimensionality for conduction depends on the localization length, the one-dimensional density of states and the bandwidth in the transverse direction. For the Li and Ag systems with $x \geqslant 0.25$, significant transport anomalies due to the order–disorder effect of M ions with a close M2–M2 distance occur at about 250 and 200 K, respectively. The magnetic properties are explained in terms of a one-dimensional Heisenberg-like model with the exchange coupling constants J_{1D} proportional to x^2.

$Li_{1+x}V_3O_8$ has two kinds of phase corresponding to the small x range ($0 \leqslant x < 1.5$) and the large x range ($x \geqslant 3$) [3], which are called the γ1- and γ2-phases, respectively. For the γ2-phase shown in figure 1(b), the Li1 ion is displaced through an octahedral face into a

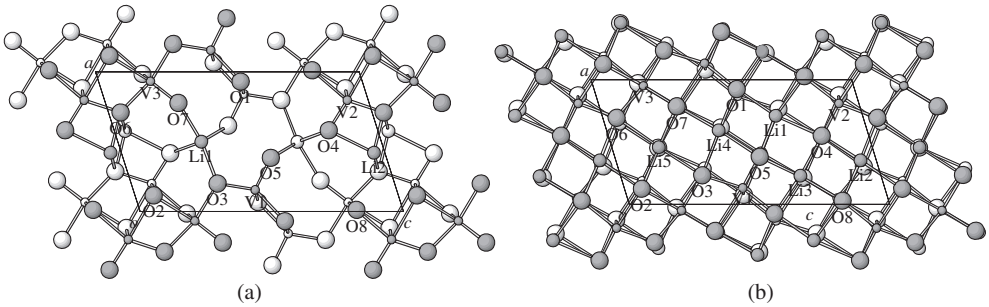

Figure 1. The crystal structures of (a) γ1-$Li_{1.29}V_3O_8$ [5] and (b) γ2-$Li_4V_3O_8$ [2] projected on the *ac*-plane, where the open circles and the shaded ones with atom-numbering denote positions at $y = 1/4$ and $3/4$, respectively. The Li2 ion in (a) is located with a probability of 0.29, while the Li4 and Li5 sites in (b) are assumed to be occupied with a total probability of $1/2$.

neighbouring octahedral site, whereas Li2 shifts its position very slightly to adopt octahedral coordination. The packing of the O ion array is adjusted slightly to adopt an arrangement that approaches cubic close-packing. $Li_4V_3O_8$ ($x = 3.0$) has a defect rock-salt structure and *all* of the Li and V ions are coordinated octahedrally [2]; the Li4 and Li5 sites are assumed to be occupied with a total probability of $1/2$. The atomic configurations and total energies of $Li_{1+x}V_3O_8$ calculated as a function of x within local-density-functional theory (LDFT), using the plane-wave pseudopotential method are consistent with the structural results described above [9].

This work is performed in order to clarify principally the local environments and the dynamics of Li ions in $Li_{1+x}V_3O_8$ for wide compositions through measurements of x-ray diffraction, magnetization and nuclear magnetic resonance (NMR). In section 2, structural properties for this system on the basis of an x-ray powder diffraction are described. In section 3, preliminary magnetization data are presented, and the local environments and the dynamics of Li ions are discussed. Section 4 is devoted to conclusions.

2. Structural properties

2.1. Sample preparation

Polycrystalline specimens of LiV_3O_8 and $Li_{1.25}V_3O_8$, and single crystals of LiV_3O_8, were prepared according to the procedure described in [5].

The electrochemical Li insertion to LiV_3O_8 was performed using a cylindrical stainless steel cell with three electrodes. Metallic Li foils were used as counter and reference electrodes. In order to prepare working electrodes, the LiV_3O_8 powder, acetylene black and polytetrafluoroethylene (PTFE) were mixed in a weight ratio of 85:5:10 and they were pressed into pellets 13 mm in diameter. 1 M of $LiPF_6$ in a propylene carbonate (PC)–dimethoxy ethane (DME) solution in a volume ratio of 50:50 was used as an electrolyte. The electrochemical measurements were done with a constant current method; for $x = 3.2, 3.3$ and 4.6, $I_c = 0.1$ mA in order to perform a gradual reaction, and for the rest, $I_c = 0.5$ mA. The concentration for inserted Li ions was calculated on the basis of the quantity of the electricity passed through the working electrode. The current was terminated when the calculated concentration agreed with the desired value. For several samples, the discharge and charge processes were examined repeatedly. The electrolyte for the specimens prepared electrochemically was removed with diethylcarbonate in the Ar atmosphere.

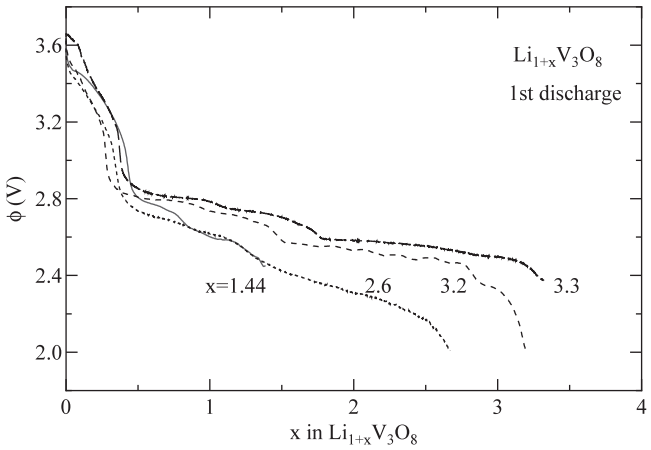

Figure 2. Examples of the first discharge curves for the Li/LiV_3O_8 electrochemical cell, where the electric current densities applied are 0.377 mA cm^{-2} for $x = 1.44$ and 2.6, and 0.0753 mA cm^{-2} for $x = 3.2$ and 3.3.

Examples of the first discharge curves or the voltages ϕ as a function of the concentration of inserted Li ions are shown in figure 2. The results are roughly similar to those reported previously [1, 3]. The concentration of inserted Li ions tends to increase for smaller current. The value $|d\phi/dx|$ for $0 \leqslant x \leqslant 0.5$ is significantly larger than that for $x > 0.5$.

2.2. Lattice constants

The x-ray powder diffraction patterns were taken at room temperature using a Rigaku RAD-IIC diffractometer with Cu Kα radiation. The composition dependence of the patterns is shown in figure 3. For the specimens prepared electrochemically, the data were obtained in vacuum to avoid decompositions in air. The single phases of $\gamma 1$ and $\gamma 2$ were confirmed for $0 \leqslant x \leqslant 1.5$ and $3.5 \leqslant x \leqslant 4.6$, respectively. For $1.5 < x < 3.5$, these phases coexist. This upper limit value for the mixed phase region is a little larger than that in [3]. The reason why the concentration of $x = 4.6$ given in figure 3 is larger than an *ideal* maximum value for the $\gamma 2$-phase is that the excess Li ions are partly intercalated in acetylene black and they partly form a small amount of another Li compound. Since these Li ions are not deintercalated, the Li concentration for the first charged state is sometimes larger than that for the initial state. The lithiation of acetylene black has also been confirmed with electron spin resonance (ESR) measurements [10].

Figure 4 indicates the composition dependences of the lattice constants with monoclinic symmetry. Here, the full and open circles indicate the present results for $\gamma 1$- and $\gamma 2$-phases, respectively, and the triangles denote the previous result for $\gamma 1$-phase [5]. The bottom of figure 4(a) shows the presence ratio of $\gamma 1$-phase to the whole phase, which is defined as $r = \left[\sum I_{\gamma 1}(hkl)\right] / \left\{\sum \left[I_{\gamma 1}(hkl) + I_{\gamma 2}(hkl)\right]\right\}$, $I_{\gamma 1(2)}(hkl)$ being the peak intensity observed for reflection (hkl) in the $\gamma 1(2)$-phase. In order to see the detail of the composition dependence, the results for the small range of x are replotted in figure 4(b). For the single $\gamma 1$-phase region, the lattice constant a has a maximum at $x \approx 0.3$; and b, c and V roughly increase with x, while β decreases. For the $\gamma 1$-phase in the mixed phase region, all of the lattice constants do not change significantly. On the other hand, the lattice constants for the $\gamma 2$-phase depend little on the composition, irrespective of the single and mixed phases.

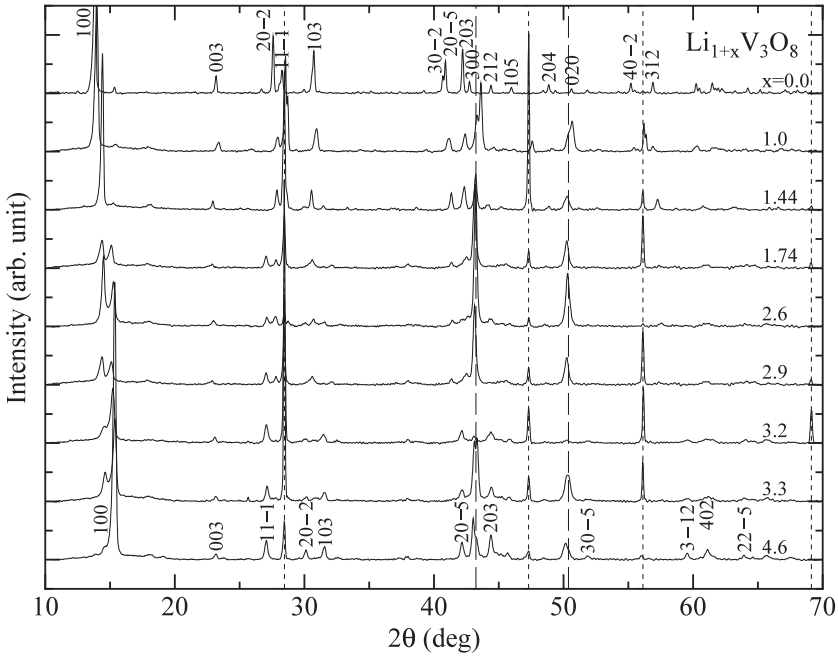

Figure 3. The composition dependence of the x-ray powder diffraction patterns for $Li_{1+x}V_3O_8$ at room temperature, where the typical Miller indices are attached for $x = 0$ (γ1-phase) and 4.6 (γ2-phase). The dotted and dashed lines show the positions for Si as a standard and those for Cu of a sample plate, respectively. For the compositions with $x \neq 0$ described here, the patterns are taken in vacuum.

As mentioned before, for Li1 and Li2 sites alone in the γ1-phase, the composition of $Li_{1+x}V_3O_8$ may be limited to $x = 0.5$ due to the strong Coulomb repulsion between the Li2 sites [6]. Therefore, the maximum phenomenon for the a-axis suggests that Li ions partly occupy another site for $x > 0.3$ as already postulated by Wadsley [11]. The LDFT calculation also supports this situation [9]. Nearly composition-independent behaviours of the lattice constants for the γ1-phase in the mixed phase and for the γ2-phase may indicate that the effective Li concentration in each phase does not change systematically with concentration for inserted Li ions. This is because the increase of effective Li concentration induces the increase of V–O bond-length for the polyhedra according to the reduction of the V valences, which gives rise to the significant increase of crystal volume. For the mixed phase, many of the inserted Li ions seem only to alter the presence ratio of each phase with optimal Li concentration.

The maximum phenomenon for the a-axis against x may be related to the initial drop of ϕ in the discharge process. For $0 \leqslant x \leqslant 0.3$, the Li ions are inserted in the Li2 site alone and the voltage is significantly correlated with the valence reduction of V ions.

3. Magnetic properties

3.1. Magnetic susceptibility

The magnetizations for the polycrystalline specimens of $Li_{1+x}V_3O_8$ with $x = 3.2$ and 4.6 obtained electrochemically, where only the latter composition indicates the single phase of γ2, were measured preliminarily by the Faraday method with a field of up to 1 T between 4.2

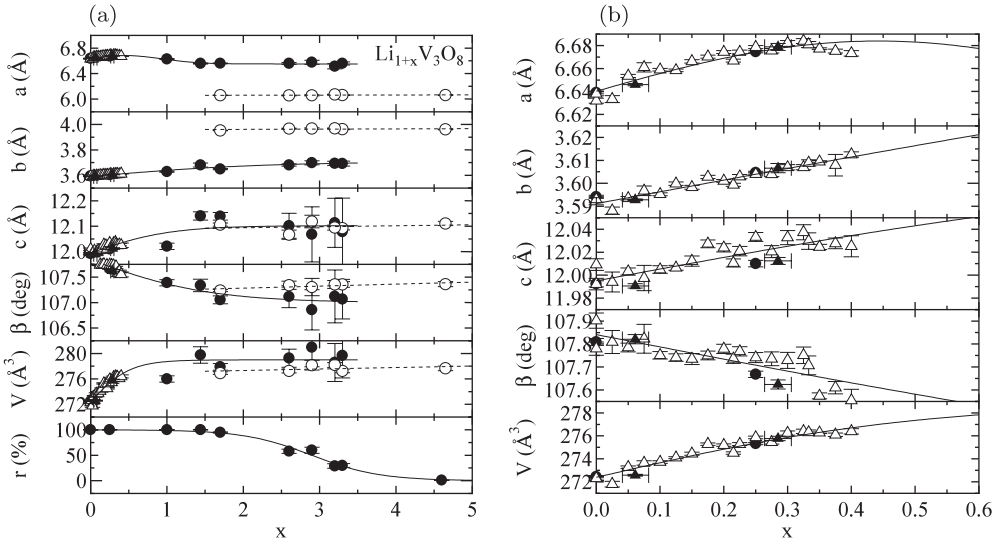

Figure 4. (a) The composition dependences of the lattice constants and the presence ratio of $\gamma 1$-phase to the whole phase for $Li_{1+x}V_3O_8$, where the full and open circles indicate the data for $\gamma 1$- and $\gamma 2$-phase, respectively, and the triangles show the previous data for the $\gamma 1$-phase. All the curves and lines are guides for the eyes. (b) The results of the lattice constants for the small range of x, where all of the curves are the same with those of (a).

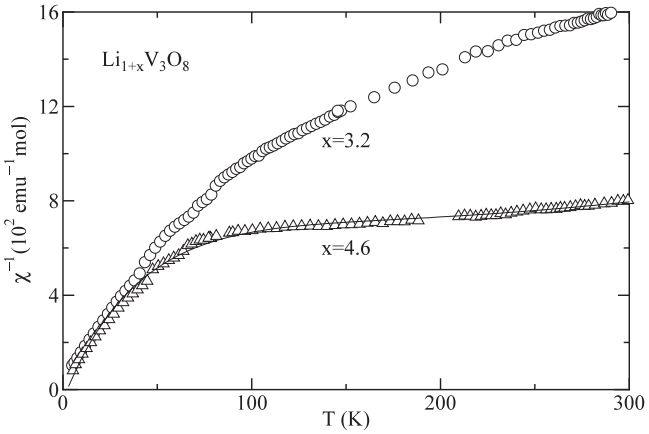

Figure 5. The temperature dependences of the inverse magnetic susceptibilities for polycrystalline specimens of $Li_{1+x}V_3O_8$ with $x = 3.2$ and 4.6, where the full curve for $x = 4.2$ indicates the result calculated from equation (1) with parameters given in text.

and 300 K. Both cooling and heating processes were examined. The magnetic susceptibility χ was deduced from the linear part of the magnetization–field curve with a decreasing field.

The temperature dependences of the inverse magnetic susceptibilities are shown in figure 5, where the results for the cooled and heated processes are the same within experimental accuracy. Both sets of data indicate small anomalies at about 40 and 65 K, which may be related to the anomalies for the NMR linewidths of Li ions described later. Above 100 K, the susceptibility with $x = 3.2$ exhibits a Curie–Weiss law-like behaviour with an apparent contribution from temperature-independent susceptibility of about 4×10^{-4} emu mol^{-1}, while

that with $x = 4.6$ indicates a weak temperature dependence. On the assumption that the one-dimensional electronic properties similar to those for the γ1-phase are still valid, in other words, only the exchange paths for the b-axis are relevant to the magnetic properties, the Heisenberg model with $W \ll U$, W and U being the bandwidth and the Coulomb repulsion energy, respectively [12], is applied to the data with $x = 4.6$. It is noted that the present specimens contain the magnetically active lithiated acetylene black, although the contribution to the intrinsic susceptibility is significantly small. Structural defects may also be inevitable for specimens prepared in the present manner. These may contribute to the Curie-like behaviour at low temperatures and sometimes mask the susceptibility maximum phenomenon for low-dimensional spin systems. Thus, the susceptibilities are described in the form

$$\chi = \chi_{1D} + \chi_{isolate} + \chi_0, \tag{1}$$

where χ_{1D} is the susceptibility for an $S = 1/2$ chain system with the parameters of the Curie constant C_{1D} and the exchange coupling J_{1D},[Note 3] $\chi_{isolate}$ is the Curie–Weiss-type susceptibility of the isolated V^{4+} ions with $C_{isolate}$ and $T_W^{isolate}$, and χ_0 corresponds to the temperature-independent susceptibility of the Van Vleck orbital and diamagnetic components. The full curve from equation (1) in figure 5 provides the following parameters: $C_{1D} = 0.67(1)$ emu K mol^{-1}, $J_{1D} = 354(6)$ K, $C_{isolate} = 0.0517(7)$ emu K mol^{-1} and $T_W^{isolate} = -2.3(3)$ K with the assumption of $\chi_0 = 0$. The number of unpaired electrons is estimated to be 2.0 per formula unit with $g \simeq 1.96$ obtained from ESR [10], which is significantly smaller than that expected from the nominal chemical formula owing to the intercalation of Li to the acetylene black and the formation of another Li compound as described before. On the other hand, the one-dimensional exchange constant is a reasonable value, since the previous work gives $J_{1D} \simeq 530x^2$ K for the intrachain [5]. Of course, in order to discuss the macroscopic magnetic properties, it is necessary to prepare purified specimens with another method and to determine the valence distribution for each composition. It is also desired to characterize transport properties for the γ2-phase in order to judge whether the localized electron model is valid or not.

3.2. Continuous-wave NMR

The continuous-wave NMR signals for the ^{7}Li nuclei in $Li_{1+x}V_3O_8$ with $x = 0$, 0.25, 2.9 and 4.6, the last two compositions being prepared electrochemically, were measured at the Larmor frequency of 15 MHz in the temperature region from 5 to 400 K using a conventional spectrometer. For all of the compositions, this method gave the single main line with nearly Gaussian lineshape. The Knight shifts have nearly zero or small negative values as will be discussed in section 3.3, which indicates that the Li atoms are ionized.

3.2.1. Quadrupolar effects. For the specimen with $x = 0$ prepared by stacking the single crystals with respect to the bc-plane, the satellites due to the quadrupolar effects at 300 K were observed for the ba^*-, bc- and a^*c-planes, a^* being perpendicular to b- and c-axes. These signals originate from the Li1 site in the γ1-phase, since the occupation for Li2 is zero or very small. The angular dependences of the interval ΔH_s between the satellites for $m = \pm\frac{3}{2} \leftrightarrow \pm\frac{1}{2}$ are shown in figure 6(a) for the ba^*- and bc-planes, and in figure 6(b) for the a^*c-plane. Here, it is noted that due to the monoclinic symmetry with $\beta = 107.8°$, the signals for the a^*c-plane are classified into two groups as shown by the open circles and crosses in figure 6(b). Generally ΔH_s has the following angular dependence:

$$\Delta H_s = H_Q(3\cos^2\theta - 1 + \eta\sin^2\theta\cos 2\phi), \tag{2}$$

[3] The Heisenberg Hamiltonian is defined as $H = \sum_{\langle i,j\rangle} J\boldsymbol{S}_i \cdot \boldsymbol{S}_j$, $\boldsymbol{S}_i$ being the spin operator at site i.

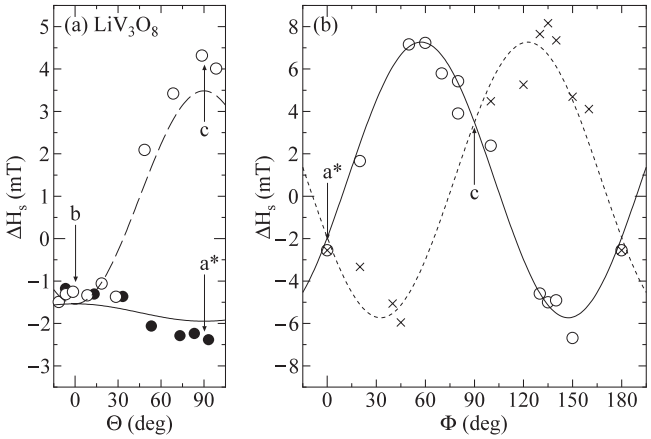

Figure 6. The angular dependences of the interval between the ^{7}Li quadrupolar satellites for $m = \pm\frac{3}{2} \leftrightarrow \pm\frac{1}{2}$ in LiV_3O_8 at 15 MHz and 300 K: (a) ba^*- and bc-plane; and (b) a^*c-plane. Here all of the curves are calculated from equation (2) with parameters given in text.

where H_Q is the quadrupole field, η is the asymmetry parameter of electric field gradient (EFG), and θ and ϕ are the polar and azimuthal angles of the magnetic field with respect to the principal axes of the EFG tensor (X, Y and Z), respectively [13]. On the basis of the data in figure 6, the quadrupole parameters are obtained as $H_Q = 3.6(1)$ mT and $\eta = 0.58(5)$; and the directions of the principal axes are determined as $\angle(Z, a^*) = 57(1)^\circ$ or 33°, and $X \parallel b$. The directions of the EFG tensor are consistent with those calculated from the point-charge model for the Li1 site using atomic parameters described in [5]. However, this model provides a small value $\eta = 0.06$ as compared with the experimental result. This discrepancy may be attributed to the small covalency effect for Li–O.

3.2.2. Dipolar effects. As described above, the main spectra for polycrystalline specimens are close to single Gaussian for all of the compositions. Since, for $x \neq 0$, the Li ions have surely several independent sites, this result suggests that the several resonance lines are superimposed and/or the *localized* motional process is significant. The temperature dependences of the peak-to-peak linewidth W of absorption derivative are shown in figure 7. Here the compositions with $x = 0$ and 0.25 correspond to $\gamma 1$-phase and that with $x = 4.6$ is $\gamma 2$-phase from the results of x-ray diffraction patterns. The linewidths for the $\gamma 2$-phase are much larger than those for the $\gamma 1$-phase. Here in this measurement, the contribution from the lithiated acetylene black may be neglected, since the Li concentration intercalated is less than 0.3 mol^{-1} of C [10, 14]. For both of the phases, the linewidths above room temperature decrease rapidly with increasing temperature, which indicates that the *long-range* motion of Li ions becomes significant, although the lineshape still remains like a Gaussian for the temperature region measured. Below room temperature, the linewidths with $x = 0$ are constant down to about 10 K, below which they exhibit a slight upturn. The results for $x = 0.25$ are almost similar to those for $x = 0$, but the former data have a slight peak at about 220 K as will be also pointed out in section 3.3. The linewidths with $x = 4.6$ are nearly temperature independent from room temperature to about 100 K, below which they increase significantly with decreasing temperature. For $x = 2.9$ with the presence ratio of the $\gamma 1$-phase $r \approx 0.5$, the resonance lines ascribed to the $\gamma 1$- and $\gamma 2$-phases should appear. However, the data are very similar to those for $x = 4.6$, which suggests that the Li signals for the $\gamma 1$-phase are masked with those for the

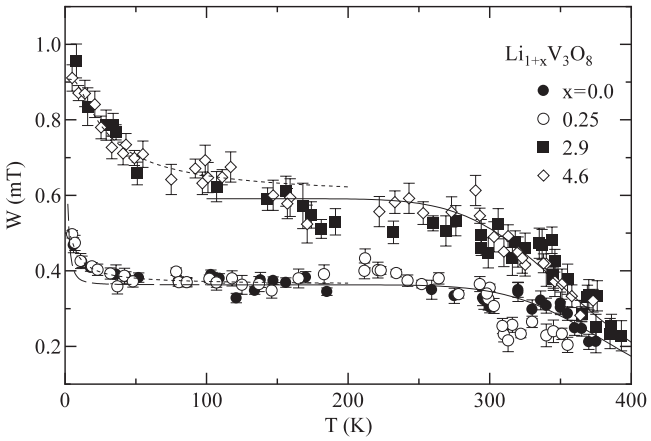

Figure 7. The temperature dependences of the peak-to-peak linewidths of absorption derivatives for ^{7}Li nuclei in $Li_{1+x}V_3O_8$ at 15 MHz, where the full (high-temperature side) and dotted (low-temperature side) curves indicate fits to equation (6), and the dashed curve is the result with a contribution from the magnetic field for powder grains.

$\gamma 2$-phase and/or the local environment around Li ions for the maximum concentration in the $\gamma 1$-phase is close to that for the $\gamma 2$-phase.

The NMR linewidths in paramagnetic materials are generally caused by several interactions between the investigated nucleus and its surroundings. The second moments from the internuclear dipolar interaction and from the magnetic field for the powder grains give significant effects for the linewidths [13, 15]. The linewidth due to the dipolar effects $\langle W\rangle_{\rm dip}$ is given by

$$\langle W\rangle_{\rm dip} = 2\sqrt{\langle M_2\rangle_{\rm Li-Li} + \langle M_2\rangle_{\rm Li-V}}, \tag{3}$$

where $\langle M_2\rangle_{\rm Li-Li(V)}$ is the second moment for Li–Li(V) pairs defined by

$$\langle M_2\rangle_{\rm Li-Li} = \frac{9}{4}\gamma_{\rm Li}^2\hbar^2\sum_k \frac{1}{r_k^6}, \tag{4}$$

$$\langle M_2\rangle_{\rm Li-V} = \frac{21}{5}\gamma_{\rm V}^2\hbar^2\sum_k \frac{1}{r_k^6}, \tag{5}$$

$\gamma_{\rm Li(V)}$, $\hbar$ and r_k being the gyromagnetic ratio of Li(V), Planck's constant and the distance between the related nuclear spins, respectively [13]. The values for $x = 0.06$, 0.29, 3 and 4 calculated based on the detailed crystal structures [2, 5] are listed in table 1.

First, the present data are analysed with the assumption that the line narrowing occurs in two stages corresponding to the temperature regions above and below 100 K. Using a formalism introduced in [16],

$$W = 1/\left[(1/B - 1/W_0)\exp(-\Delta/T) + 1/W_0\right], \tag{6}$$

where B is a temperature-independent linewidth, W_0 is the rigid-lattice linewidth and Δ is an activation energy, the results listed in table 2 are obtained from the dotted and full curves in figure 7. Here W_0 for the high-temperature side above 100 K is assumed to agree with B at low temperatures in order to reduce the number of parameters. At high temperatures, all of the compositions have $\Delta \approx 3\times 10^3$ K, which may be responsible for the long-range motion of Li ions. A similar activation energy has been reported for $Li_{1.1}V_3O_{7.9}$ [17]. At low temperatures for the $\gamma 1$-phase, the Δ values are smaller than 10 K and the W_0 ones are significantly larger

Table 1. The composition dependence of the powder-averaged linewidths $\langle W\rangle_{\rm dip}$ (mT) calculated on the basis of the dipolar interaction for the rigid lattice. For $x \leqslant 0.29$ and $x \geqslant 2$, the structural results in [5] and [2] are used, respectively.

x	Li1	Li2	Li3	Li4	Li5	$\langle W\rangle_{\rm dip}$
0.06	1	0.06	—	—	—	0.267
0.29	1	0.29	—	—	—	0.335
2	1	1	1	0	0	0.749
3	1	1	1	1	0	0.972
3	1	1	1	0.5	0.5	0.983
3	1	1	1	0	1	0.994
4	1	1	1	1	1	1.19

Table 2. Results of the analysis for the narrowing of Li NMR linewidth in $Li_{1+x}V_3O_8$.

	Low temperatures			High temperatures	
x	B (mT)	Δ (K)	W_0 (mT)	B (μT)	Δ (10^3 K)
0.0	0.363(2)	9(1)	0.51(2)	0.03(7)	3.7(7)
0.25	0.364(8)	5(4)	0.62(19)	0.08(16)	3.1(6)
2.9	0.57(10)	31(18)	0.95(6)	0.3(3)	2.9(3)
4.6	0.59(2)	31(5)	0.90(1)	0.2(2)	3.0(4)

than $\langle W\rangle_{\rm dip}$. They indicate the narrowing model in two stages to be inadequate and another contribution from the magnetic field for powder grains should be considered. This contribution is given by $2.3 \times 10^{-3}(\chi H_0)^2$, where H_0 is the resonance field, from the model proposed in [15] with the assumption of cubic close packing of spherical particles. The dashed curve for $x = 0$ in figure 7 is the result calculated based on this model. The upturn behaviour at low temperatures is roughly explained. Therefore the linewidths below room temperature for the $\gamma 1$-phase are basically regarded as the dipolar widths for the rigid lattice. On the other hand, the low-temperature behaviour for the $\gamma 2$-phase seems to provide Δ values reasonable for the narrowing model in two stages. For $x = 2.9$ and 4.6, the linewidths at the lowest temperature agree roughly with the dipolar widths in table 1 considering that the numbers of unpaired electrons may range from 2 to 3 on the basis of the susceptibility results; that is, the Li ions are ordered at the lowest temperature. The narrowing behaviour at the low-temperature side seems to be correlated with the susceptibility anomalies described before. The order–disorder effect of Li ions may cause a slight change of superexchange coupling.

The correlation times for the long-range motion of Li ions for $x = 0$ and 0.25 estimated by [18, 13]

$$\tau_{\rm m} \simeq \frac{4\ln 2}{\gamma_{\rm Li}\pi W}\tan\left\{\frac{\pi}{2}\left(\frac{W}{W_0}\right)\right\}, \tag{7}$$

with W_0 equal to B at low temperatures are $\tau_{\rm m} \simeq 0.12$ and 0.071 ms at 400 K, respectively. The corresponding self-diffusion coefficients are calculated as $D \simeq 5.6 \times 10^{-12}$ and 9.2×10^{-12} cm^2 s^{-1} from the relation [13]

$$D = \frac{l^2}{n\tau_{\rm m}}, \tag{8}$$

where the hopping distance l and the number of near neighbouring sites n are taken as 3.6 Å and 2, respectively. These values are one order of magnitude smaller than those obtained from

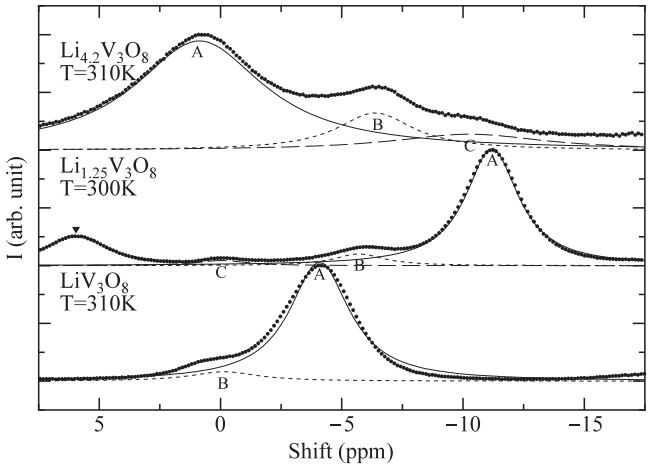

Figure 8. The composition dependence of the MAS-NMR central spectra for the ^{7}Li nuclei in $Li_{1+x}V_3O_8$ at 233.23 MHz, where all of the curves indicate a decomposition to symmetric Lorentzians. The triangle for $x = 0.25$ shows the spinning side band position.

galvanostatic intermittent titration and pulse polarization methods, although the activation energies are similar to each other [3]. This discrepancy would be reconciled in terms of the thermodynamic correction factor in the so-called Darken equation [19], which is estimated from the slope of the titration curve.

3.3. Magic-angle spinning NMR

The MAS-NMR spectra for the ^{7}Li nuclei in $Li_{1+x}V_3O_8$ with $x = 0$, 0.25 and 3.2, the last composition being prepared electrochemically, were recorded on Bruker Avance spectrometers at 233.23 and 116.61 MHz in the temperature region between 240 and 390 K. Spinning speeds from 4 to 7 kHz were used and all of the spectra were referenced to LiCl solution at 0 ppm. The spin-lattice relaxation time T_1 was obtained with the inversion–recovery measurements.

Examples of the central spectra are shown in figure 8. They are decomposed to two or three Lorentzians as indicated by full, dashed or dotted curves assuming axial or isotropic contributions for the shift. Here, it should be noted that for Li1 with $x = 0$, the second-order quadrupole shift of the centre of gravity [20] is -0.0074 ppm at 233.23 MHz and the anisotropic pattern width is at most 0.018 ppm, so this effect for the spectra can be neglected.

For $x = 0$, there exist two resonance lines named A and B. Using the relative intensity for each line, the Li concentrations normalized to the nominal value against temperature are estimated as shown in figure 9(a). Here, the relative intensity for the spinning side bands is assumed to be the same with that for the central line. The Li concentrations do not depend on temperature, and the A- and B-lines may be attributed to the signals from Li1 and Li2 sites, respectively, since the Li2 ion appears to exist slightly even when the nominal concentration is fixed at $x = 0$ [5]. Note that the slight occupation of Li2 gives rise to unpaired spins for V ions.

The temperature dependences of the shifts and the spin-lattice relaxation times for $x = 0$ are indicated in figures 9(b) and (c), respectively. The shift for Li2 is almost zero, but that for Li1 increases negatively with decreasing temperature. The latter result may correspond to a sum of the hyperfine shift via the Fermi contact interaction and temperature-independent

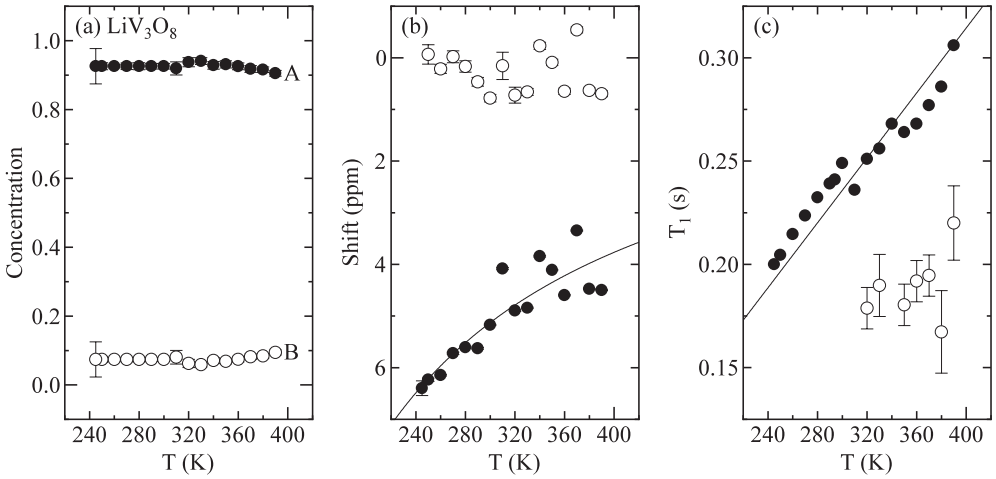

Figure 9. The temperature dependences of (a) the Li concentrations normalized to the nominal value; (b) the shift; and (c) the spin-lattice relaxation times for ^{7}Li nuclei in LiV_3O_8, where the full curve in (b) and the full line in (c) indicate fits to equations (9) and (10), respectively.

terms. The hyperfine shift δ depends linearly on the magnetic susceptibility,

$$\delta = \frac{H_{\rm hf}}{N\mu_{\rm B}}\chi, \tag{9}$$

where $H_{\rm hf}$ is the hyperfine field, N is the number of magnetic V ions and $\mu_{\rm B}$ is the Bohr magneton. The full curve in figure 9(b) based on the previous data of the magnetic susceptibility [5] provides $H_{\rm hf} = -26(3)$ mT $\mu_{\rm B}^{-1}$. The origin of the negative $H_{\rm hf}$ value or the spin transfer mechanism in the present system may originate from spin polarization effects due to the exchange interactions [21].

T_1 for Li1 with $x = 0$ is linear in temperature, which suggests that the relaxation is of the quadrupole type for the rotational motion of Li ions. With the extreme narrowing condition and the nuclear spin $I = \frac{3}{2}$, this is written by [13]

$$1/T_1^{\rm Q} = \frac{1}{10}\left(1 + \frac{\eta^2}{3}\right)\left(\frac{e^2qQ}{h}\right)^2 \tau_{\rm c}, \tag{10}$$

where $\tau_{\rm c}$ is an effective correlation time for the motion and it is proportional to the inverse of temperature. The full line in figure 9(c) and the quadrupole parameters for Li1 described before lead to $\tau_{\rm c} \simeq 7.9 \times 10^{-7}/T$ s. T_1 for Li2 seems to have a temperature dependence similar to that for Li1, although it is difficult to get the precise result due to the poor intensity. It is not necessary to consider the hyperfine interaction for the main relaxation mechanism, since the relaxation rates of the A-line for the different compositions are similar to that for $x = 0$ as will be described below.

The MAS-NMR results for $x = 0.25$ are shown in figure 10. Three resonance lines (A, B and C) exist above 270 K, and at 260 K, the D-line with more negative shift appears. At the lower temperature, it is difficult to distinguish between the B- and C-lines. At first sight, the presence of three kinds of Li ions seems to be inconsistent with the x-ray study for $x = 0.29$, which indicates only two kinds of Li environments. However, the Li concentration for the C-line with zero shift is too small (<0.05) to be detected from the x-ray structure analysis. Thus, the A- and B-lines originate from the Li1 and Li2 sites, respectively, and the C-line may come from another tetrahedral Li site postulated by Wadsley [11]. Since the V ion is

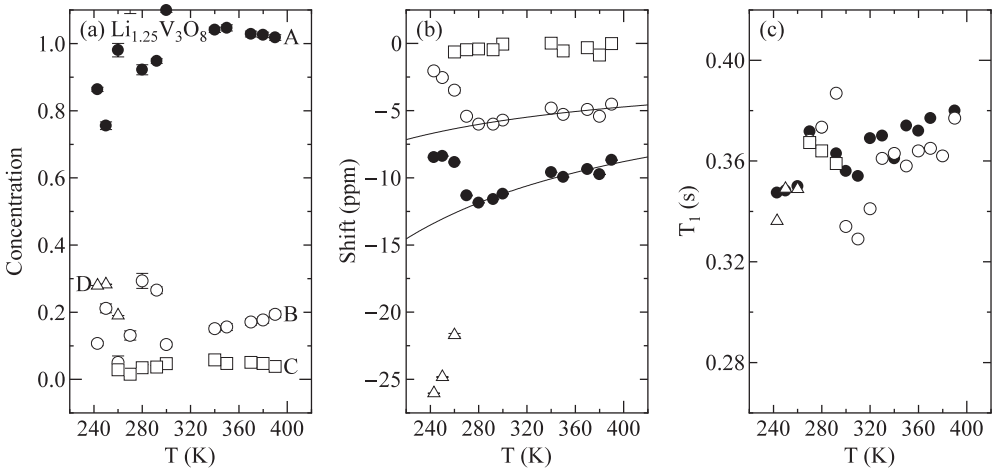

Figure 10. The temperature dependences of (a) the Li concentrations normalized to the nominal value; (b) the shift; and (c) the spin-lattice relaxation times for ^{7}Li nuclei in $Li_{1.25}V_3O_8$, where the full curves in (b) indicate fits to equation (9).

more reduced and the compound is more magnetic as compared with those for $x = 0$, the hyperfine shifts for the Li1 and Li2 ions increase more negatively. The full curves for Li1 and Li2 in figure 10(b) provide $H_{hf} = -21(2)$ and $-9(2)$ mT μ_B^{-1}, respectively, with equation (9). Below 260 K, these shifts show opposite temperature dependences and the shift for the D-line increases negatively. This result, as well as the small peak of the Li linewidth presented before, suggests the occurrence of a phase transition for the local environments of Li.

The T_1s for $x = 0.25$ are the same order as those for $x = 0$, but their temperature dependences are weak. This may be due to an increase of the temperature-independent contribution from the exchange-coupled V ions [22] via a transferred hyperfine interaction. There exist small anomalies above 260 K, at which the local environments of Li change.

Figure 11 indicates the MAS-NMR results for $x = 3.2$. Since this nominal composition corresponds to the $\gamma 2$-phase for which the quadrupole parameters are not determined, it is not clear whether the line decomposition in figure 8 is reasonable. The comparison between the spectra at 233 and 116 MHz at room temperature indicates a line broadening for the lower Larmor frequency, suggesting that the quadrupole frequency is larger than that for the $\gamma 1$-phase. Unfortunately, it is difficult to get precise quadrupole parameters from this result alone, since there are several crystallographically independent sites for Li. It should be also noted that this specimen has the acetylene black containing Li ions. Our preliminary MAS-NMR measurements for Li ions doped directly to the acetylene black without active $Li_{1+x}V_3O_8$ indicate that, at room temperature, the shift with symmetric lineshape is zero and the T_1 is of the order of 10^0 s. Therefore, the Li concentrations normalized to the nominal value shown in figure 11(a), obtained taking no account of the lithiation of acetylene black, are speculative.

There are apparently three resonance lines (A, B and C) above 310 K, where a part of the A-line may come from the Li ions in acetylene black judging from the shift and T_1. Below 310 K, a new D-line is added, which is attributed to the change in the local environment of Li ions likely due to their orderings. At the same temperature, the lines with negative shifts are accompanied with a significant jump, as indicated in figure 11(b). The shift for the B-line at the high-temperature side increases negatively with increasing temperature, which is not simply understood with a constant hyperfine coupling in equation (9).

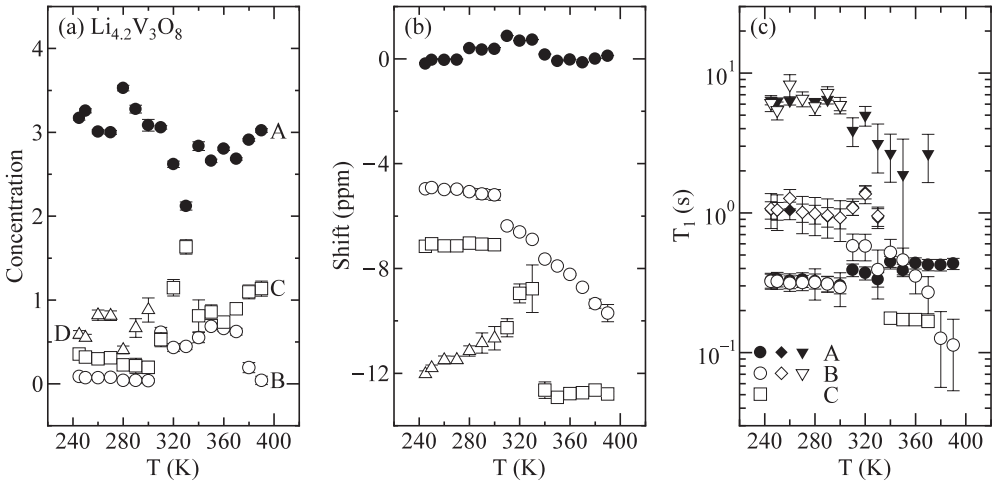

Figure 11. The temperature dependences of (a) the Li concentrations normalized to the nominal value; (b) the shift; and (c) the spin-lattice relaxation times for ^{7}Li nuclei in $Li_{4.2}V_3O_8$.

The nuclear magnetizations for the A- and B-lines do not exhibit a single exponential recovery; there seem to exist three kinds of relaxation as shown in figure 11(c). Several components for T_1s strongly depend on temperature above 310 K, while below it, all of the T_1s are almost temperature independent. Since the T_1s for $x = 0$ and 0.25 do not show large site dependences and that for the lithiated acetylene black is rather long, as mentioned above, it is natural to consider that several kinds of T_1s are attributed to the presence of Li ions located in the cathode and the acetylene black, and the boundary between these substances. In order to explore the local properties for Li ions in $Li_{1+x}V_3O_8$ quantitatively, it is highly desired to prepare acetylene black-free lithiated specimens.

4. Conclusions

The structural properties for $Li_{1+x}V_3O_8$ with nominal compositions of $0 \leqslant x \leqslant 4.6$ prepared electrochemically indicate that the $\gamma 1$-phase with the octahedral (Li1) and tetrahedral (Li2) coordinations for the Li sites appears in $0 \leqslant x \leqslant 1.5$ as a single phase and the $\gamma 2$-phase with the octahedral coordination alone is in $x \geqslant 3.5$. For $1.5 < x < 3.5$, these phases coexist, accompanied with a change of the presence ratio. The nominal concentration that exceeds the maximum value for the $\gamma 2$-phase indicates the partial intercalation of Li ions to acetylene black and the formation of a small amount of another Li compound.

The electronic properties are revealed through measurements of magnetization and NMR for ^{7}Li. Application of the one-dimensional chain model established for the $\gamma 1$-phase to the susceptibility data with $x = 4.6$ provides reasonable results for the Li concentration and the exchange constant. For $x = 0$, the quadrupole parameters are determined precisely. The analyses of NMR linewidths for the $\gamma 1$- and $\gamma 2$-phases indicate that the activation energies for the long-range motion of Li ions are about 3×10^3 K. For the $\gamma 1$-phase, the Li ions form a rigid lattice below room temperature, while for the $\gamma 2$-phase, they become ordered at very low temperature. The latter property may be favourable for the performance of a secondary battery.

MAS-NMR spectra for the $\gamma 1$-phase clearly reflect the site differentiation for Li; the Li1 shift originates from a negative spin transfer, while the effect for Li2 and another site is less significant. The spin-lattice relaxation for $x = 0$ is explained with the quadrupole

interaction mechanism. For $Li_{1.25}V_3O_8$ with variable-range hopping-type transport anomalies at $T_c \simeq 250$ K, the phase transition for the Li local environments occurs at the corresponding temperature. The spectra for the $\gamma 2$-phase are different from those for the $\gamma 1$-phase, and the complicated relaxations likely originating from Li ions located in the cathode and the acetylene black, and the boundary between these substances, are detected.

References

[1] Pistoia G, Pasquali M, Tocci M, Moshtev R V and Maner V 1985 *J. Electrochem. Soc.* **132** 281
[2] de Picciotto L A, Andendorff K T, Liles D C and Thackeray M M 1993 *Solid State Ion.* **62** 297
[3] Kishi T, Kawakita J and Miura T 2000 *Electrochemistry* **68** 2 and references therein
[4] Onoda M and Kanbe K 2001 *J. Phys.: Condens. Matter* **13** 6675
[5] Onoda M and Amemiya I 2003 *J. Phys.: Condens. Matter* **15** 3079
[6] Onoda M 2004 *J. Phys.: Condens. Matter* **16** 8957
[7] Gustafsson T, Thomas J O, Koksbang R and Farrington G C 1992 *Electrochem. Acta* **37** 1639
[8] Onoda M, Ohki T and Uchida Y 2004 *J. Phys.: Condens. Matter* **16** 7863
[9] Benedek R and Thackeray M M 1999 *Phys. Rev.* B **60** 6335
[10] Onoda M and Mutoh T 2004 unpublished results
[11] Wadsley A D 1957 *Acta Crystallogr.* **10** 261
[12] Bonner J C and Fisher M E 1964 *Phys. Rev.* A **3** 640
[13] See, for example, Abragam A 1963 *The Principles of Nuclear Magnetism* (Oxford: Oxford University Press)
[14] Nakamura M, Imaki K, Uchimoto Y and Wakihara M 2002 *J. Phys. Chem.* B **106** 6437
[15] Drain L E 1962 *Proc. Phys. Soc. Lond.* **80** 1380
[16] Hendrickson J R and Bray P J 1973 *J. Magn. Reson.* **9** 341
[17] Halstead T K, Benesh W U, Gulliver R D II and Huggins 1973 *J. Chem. Phys.* **58** 3530
[18] Kubo R and Tomita K 1954 *J. Phys. Soc. Japan* **9** 888
[19] See, for example, Crank J 1975 *The Mathematics of Diffusion* (Oxford: Clarendon)
[20] See, for example, Man P P 1997 *Phys. Rev.* B **55** 8406
[21] Carlier D, Ménétrier M, Grey C P, Delmas C and Ceder G 2003 *Phys. Rev.* B **67** 174103
[22] Moriya T 1956 *Prog. Theor. Phys.* **16** 641